In Situ Investigation of High-Pressure Hydrogen-Induced Swelling in Elastomers and Its Correlation with Material Properties

Wenbin Kuang [a, *], Ethan K. Nickerson [a], Yongsoon Shin [b], M. F. N. Taufique [a], Dustin T. Clelland [a], Robert J. Seffens [a], and Kevin L. Simmons [a, *]

[a] *Energy and Environment Directorate, Pacific Northwest National Laboratory, Richland, Washington 99354, USA*

[b] *Physical and Computational Science Directorate, Pacific Northwest National Laboratory, Richland, Washington 99354, USA*

* Corresponding emails: wenbin.kuang@pnnl.gov; kl.simmons@pnnl.gov

In Situ Investigation of High-Pressure Hydrogen-Induced Swelling in Elastomers and Its Correlation with Material Properties

ABSTRACT

The resistance of elastomeric materials to high-pressure hydrogen-induced damage is essential for ensuring the reliability of hydrogen infrastructure. In this study, we systematically investigated the swelling behavior and hydrogen transport properties of four elastomer types – EPDM, NBR, FKM, and HNBR – using a custom in-situ view cell system capable of real-time monitoring during decompression from pressures up to 96.5 MPa. Each elastomer was formulated with and without fillers and plasticizers to assess the effects of formulation on swelling response. Thermal desorption analysis (TDA) was employed to determine equilibrium hydrogen content and diffusion coefficients, providing insight into gas uptake and mobility within each material. Correlation analyses using Pearson and Spearman coefficients revealed that the diffusion coefficient showed a stronger relationship with swelling behavior than hydrogen content, highlighting the dominant role of hydrogen mobility. Filled elastomers, particularly those with carbon black, consistently showed reduced swelling due to enhanced stiffness and reduced diffusivity. These results deepen our understanding of diffuso-mechanical interactions in elastomers and support the rational design of sealing materials for high-pressure hydrogen systems.

Key Words: In-situ elastomer swelling measurement; EPDM; NBR; FKM; HNBR; High-Pressure Hydrogen.

INTRODUCTION

The global transition toward alternative energy solutions is driven by the need for energy abundance, resilience, and affordability. To ensure a stable and reliable energy future, policymakers and researchers are prioritizing the development of new energy technologies that enhance both energy security and economic feasibility. Among these, hydrogen emerges as a promising solution due to its potential to serve as a scalable, reliable, and efficient energy carrier. [1,2] Hydrogen offers significant advantages due to its high energy density and versatility. It can be produced from abundant resources, including water through electrolysis powered by renewable energy and natural gas reforming with or without carbon capture. [3,4] However, the widespread adoption of hydrogen faces challenges related to production costs, infrastructure development, storage and transportation, and safety. Hydrogen's deleterious interaction with conventional materials necessitates advancements in engineering solutions to ensure cost-effective and durable deployment.

A major hurdle in hydrogen infrastructure is the degradation of materials exposed to high-pressure hydrogen environments. [5-7] Metallic components are susceptible to embrittlement, while polymer-based sealing materials experience mechanical failures such as explosive decompression failure. These issues can compromise system efficiency and reliability and are mitigated by expensive operation & maintenance (O&M) requirements. This highlights the need for resilient material solutions that can safely maintain performance under extreme conditions, thereby decreasing O&M costs. In hydrogen infrastructure, elastomers play a crucial role in sealing components such as O-rings and gaskets. However, under high-pressure hydrogen conditions, these components are prone to premature failure. The primary issue is excessive swelling due to hydrogen absorption, followed by rapid gas expansion upon depressurization. This process can

lead to blistering and extrusion fractures, ultimately compromising seal integrity. [8,9] Therefore, understanding the real-time behavior of elastomers under these conditions is essential to developing more resilient materials and improving hydrogen system reliability. *In situ* measurements are crucial for capturing the dynamic interactions between hydrogen and elastomeric materials under actual operating conditions. Unlike *ex situ* methods, which provide only post-exposure snapshots and may fail to capture transient effects, *in situ* techniques allow continuous monitoring of swelling kinetics, hydrogen diffusion behavior, and failure progression.

Alvine *et al.* [10] made a notable advancement by designing a unique tensile testing system that functions inside an autoclave, enabling *in situ* mechanical evaluation of thin polymer samples in hydrogen atmospheres at pressures up to 35 MPa with an upper operating temperature 100°C. Due to space constraints, the maximum load and displacement are limited at 530 N and <100 mm, respectively. Castagnet *et al.* [11] integrated a hydraulic testing machine within a pressurized hydrogen chamber to examine the long-term creep and ductile fracture behavior of polyethylene and polyamide 11, with testing pressures constrained to 3 MPa in compliance with gas distribution standards. Along the same lines, Wang *et al.* [12] developed an *in-situ* setup for conducting spiral notch torsion tests in hydrogen at pressures up to approximately 15 MPa, thereby reducing the specimen size effect in assessing the fracture toughness and fatigue properties of pipeline materials. Complementary progress was achieved with the development of a specialized *in situ* tribology tester [13–15], which facilitated the measurement of friction and wear in acrylonitrile butadiene rubber (NBR) and ethylene propylene diene monomer (EPDM) under hydrogen pressures as high as 27.6 MPa. Theiler *et al.* [16] explored the fretting behavior of crosslinked hydrogenated NBR (HNBR), NBR, and EPDM when paired with 316L stainless steel in hydrogen environments up to 10 MPa. Their work identified a gross slip regime for all rubbers studied and showed that friction

in HNBR and EPDM increased with pressure. Additionally, they found that carbon black (CB)-containing HNBR experienced primarily adhesive wear, while the introduction of polyamide fillers notably reduced wear rates. Another study [17] examined the tribological performance of NBR in hydrogen environments at pressures below 10 MPa using a custom-designed tribometer, revealing that higher silica loading significantly reduced both wear and friction. Hydrogen transport properties represent another important consideration for polymer sealing materials used in high-pressure hydrogen environments. Jung et al. [18] reported the development of a nondestructive impedance spectroscopy technique capable of providing *in situ* and real-time quantification of hydrogen ingress and desorption in rubber materials exposed to hydrogen gas at pressures up to 10 MPa. This method enables the simultaneous evaluation of both hydrogen diffusion and desorption behavior and offers a valuable complement to *ex situ* techniques such as thermal desorption analysis (TDA). More recently, an *in situ* high-pressure permeation measurement system was established to characterize the hydrogen transport properties of carbon black-filled EPDM across a pressure range of 1 to 10 MPa. The study revealed a decline in both hydrogen permeability and diffusivity with increasing pressure, while solubility remained largely unaffected. [19] Collectively, these studies underscore the critical importance of conducting *in situ* measurements under hydrogen gas to ensure the accuracy and relevance of material performance data.

Further insights were provided by Kane-Diallo *et al.* [20], who introduced a high-pressure experimental setup that combines a hydraulic tensile system with a pressure vessel capable of reaching 40 MPa and 150°C. An important innovation in this system is an optical window that permits direct visualization of hydrogen-polymer interactions and morphological transitions during decompression. Similarly, Ono *et al.* [21] employed a pressure-resistant apparatus featuring

a sapphire sight window to observe EPDM compounds during hydrogen pressure cycling up to 15 MPa. Their analysis revealed that material degradation in EPDM is driven by complex coupled diffusion-mechanical effects rather than simple cavity growth and merging. Subsequent research [22,23] examined cavity initiation and evolution in filler-free EPDM using both 2D optical techniques and 3D *in situ* tomography during cyclic exposure to 15 MPa hydrogen. These studies found that pressure cycling led to fewer but larger cavities, and that not completely removing pressure between cycles effectively mitigated damage accumulation. To extend these investigations to higher pressure regimes, we developed a novel *in situ* view-cell platform capable of evaluating swelling behavior in HNBR under hydrogen pressures up to 96.5 MPa [24]. Our findings revealed a non-linear volume response during rapid decompression of high-pressure hydrogen, with the most significant expansion occurring as pressure dropped below 10 MPa and continuing even after complete depressurization. These findings underscore the importance of time-dependent effects in hydrogen-induced polymer responses and highlight the limitations of *ex situ* or postmortem evaluations. Nevertheless, a significant gap remains: there is a critical need for comparative *in situ* studies across a broader range of elastomer formulations under consistent testing conditions to better elucidate their performance in hydrogen-rich environments.

In this study, we systematically investigated four elastomer types – EPDM, NBR, FKM, and HNBR – using our previously reported *in situ* view cell test system [24]. Each elastomer type included variants incorporating fillers and/or plasticizers to evaluate the impact of these additives on swelling behavior during rapid decompression from high-pressure hydrogen. By comparing the swelling responses both within and across material types, we aimed to develop a comprehensive understanding of how different elastomers interact with high-pressure hydrogen gas. To assess hydrogen transport properties, we employed thermal desorption analysis (TDA) [25-27], a well-

established technique for quantifying gas penetration and diffusion in materials. This method enabled us to determine key parameters such as equilibrium hydrogen content—defined as the maximum concentration of hydrogen absorbed by the material when exposed to a given pressure and temperature over sufficient time—and diffusion coefficients under controlled hydrogen exposure conditions. By correlating these transport properties with swelling test results, we gained deeper insights into the role of hydrogen diffusion and the influence of fillers on elastomer swelling behavior. To further elucidate structure–property relationships, we performed correlation analyses between material properties and swelling behavior using both Pearson and Spearman correlation coefficients. This dual statistical approach captured both linear and monotonic trends, providing integrative insights into how formulation variables and hydrogen transport characteristics influence swelling.

MATERIALS AND METHODS

Materials

We procured four elastomer types from Takaishi Industries: EPDM, NBR, FKM, and HNBR. Each material type includes variants formulated with plasticizers and/or fillers to assess the effects of these additives on elastomer swelling behavior under extreme hydrogen conditions. All samples were received as 15 × 15 cm sheets. Detailed compositions of these model elastomers are summarized in Tables 1, 2, and 3. The material properties of the model elastomers are also showed in Table 4. Cylindrical specimens measuring 10 mm in diameter and approximately 3 mm thick were punched from the sheets. To maintain consistent testing conditions, the specimens were kept in a desiccator at room temperature for more than 168 h prior to testing. For

digital image correlation (DIC), a speckle pattern was created by first applying a white base coat, followed by a layer of black speckles using spray paint. This high-contrast speckle pattern enables tracking and analysis of speckle movement between frames to calculate full-field surface displacements and strains with high spatial resolution.

High-Pressure Hydrogen Testing

All model elastomer specimens were exposed to >99.9% purity hydrogen gas using a series of 5-mL pressure vessels (acquired from High-Pressure Equipment). These pressure vessels were flushed and purged sufficiently with argon gas for safety considerations. The pressure cycling protocol consisted of four stages: (1) an initial rapid pressurization to around 13 MPa (gas supply bottle pressure), followed by a ramp-up to 90 MPa within 2 min using a Haskel hydrogen gas booster (model AGT-62/152); (2) a pressure hold at 90 MPa overnight (>20 h) to ensure saturation; (3) a controlled pressure release down to atmospheric pressure at a rate of approximately 8 MPa/min; and (4) a stabilization phase at ambient pressure lasting up to 4 h. Throughout the entire procedure, high-resolution images were continuously acquired using the DIC system to monitor the volume change of the elastomer samples.

Evaluation of Elastomer Swelling

The evaluation method of elastomer volume change was described in our prior work [24] and applied in this study. Vic-2D software (Correlated Solutions, Inc., 2010) was utilized with a subset size of 41 pixels and a step size of 14 pixels. A filter size of 15 was applied to smooth the displacement data. Principal strain values were calculated and averaged over the visible area of

each specimen. The averaged principal strain was then used to estimate volumetric changes during the entire course of testing, under the assumption of isotropic expansion. Pressure measurements were correlated with volume data using corresponding timestamps to ensure temporal alignment.

Thermal Desorption Analysis (TDA)

To assess the hydrogen transport behavior of the model elastomers, thermal desorption analysis (TDA) was carried out. Our TDA setup has a 25.4-mm diameter Swagelok tube housed within a temperature-controlled oven (volume: 64 L). This apparatus was connected to a gas chromatograph (purchased from Infico) equipped with an automated gas sampling system. Argon served as the carrier gas, flowing through the Swagelok tube at a rate of 50 mL/min to convey the desorbed hydrogen to the GC. The oven was maintained at a constant 30 °C throughout the test. The GC samples hydrogen released from the specimen every 5 min and analyzes over a 1-minute period to determine hydrogen concentration. The desorption experiment was performed over a total duration of 24 h. Assuming no significant fluctuation in desorption rate within each 5-minute interval, the hydrogen concentration in the sample at a given time t, denoted C_t, was calculated using the following:

$$C_t = \frac{32}{\pi^2} C_0 \left[\sum_{n=0}^{\infty} \frac{exp^{(-(2n+1)^2 \pi^2 Dt/z^2)}}{(2n+1)^2} \right] \left[\sum_{n=1}^{\infty} \frac{exp^{(-D\beta_n^2 t/r^2)}}{\beta_n^2} \right]$$

where C_t is the remaining hydrogen content (wt. ppm), D is the (non-equilibrium [28,29]) diffusion coefficient (m^2/s), z is the sample thickness, r is the sample radius, β_n represents the roots of the zero-order Bessel function, with the first six roots given as: $\beta_1 = 2.405$, $\beta_2 =$

5.5204, $\beta_3 = 8.654$, $\beta_4 = 11.792$, $\beta_5 = 14.931$, and $\beta_6 = 18.071$.[30] The hydrogen equilibrium concentration and diffusion coefficient were determined by fitting the diffusion equation to experimental data, treating the initial hydrogen content and the zero-time diffusion coefficient as fitting parameters. [31-33]

Correlation Analysis of Elastomer Properties and Swelling Behavior

To investigate the relationship between elastomer properties and their swelling behavior, both Pearson and Spearman correlation coefficients were calculated, offering complementary insights into linear and monotonic associations. [34]

Pearson Correlation Coefficient (r): This coefficient quantifies the strength and direction of the linear relationship between two continuous variables. It is calculated as:

$$r = \frac{\sum(x_i - \bar{x})(y_i - \bar{y})}{\sqrt{\sum(x_i - \bar{x})^2 \sum(y_i - \bar{y})^2}}$$

where x_i and y_i are the individual sample values, and $\bar{x}$ and $\bar{y}$ are their respective means.

Spearman Correlation Coefficient (ρ): This nonparametric measure evaluates the strength of a monotonic relationship between two variables, based on rank-order. It is calculated as:

$$\rho = 1 - \frac{6\sum d_i^2}{n(n^2 - 1)}$$

where d_i is the difference between the ranks of corresponding values and n is the total number of observations.

Correlation coefficients were computed and visualized for both filled and unfilled elastomers. The results revealed distinct patterns in how various material properties correlate with swelling behavior, depending on the presence of fillers. Pearson's coefficient highlighted linear trends, while Spearman's coefficient captured more general monotonic relationships, including potential nonlinear interactions. This dual-analysis approach provides a more nuanced understanding of structure–property–swelling relationships in elastomers, informing the rational design and formulation of materials with tailored swelling responses.

RESULTS AND DISCUSSION

To ensure a consistent basis for evaluating and comparing swelling behavior, all model elastomers were subjected to the same pressure cycle (Figures S1-S5), from initial pressurization through the pressure-holding phase to subsequent depressurization, as detailed in the *High-Pressure Hydrogen Testing* section. Sample volumes were normalized to their initial values at the start of the test. Slight variations in peak pressure were observed across all tests, ranging from 86 to 94 MPa. These fluctuations were primarily due to the small volume of the view cell sample chamber (~3.2 cm^3) and the pressurization mechanics, which depend on the gas booster's stroke action. However, this ~4% deviation from the target pressure is expected to have a negligible impact on the results. During the pressurization phase, all model elastomers exhibited an approximate volume contraction of 2-3% due to external pressure-induced compression (Figures S1b, S2b, S3b, S4b, and S5b). This contraction partially or fully recovered within 2 hours for EPDM, NBR, and HNBR as hydrogen diffused into the rubber matrix and reached saturation. In contrast, recovery took approximately 7-10 hours for the two FKM sets, likely due to their relatively low diffusion coefficients, as shown in Figure 1b (more detail available in

Table S1). Other contributing factors, such as bulk modulus, filler loading, and crosslink density, may also play a role in this delayed response. Additionally, we found that incorporating CB filler led to a higher hydrogen equilibrium content for both EPDM and NBR compared to unfilled systems or those filled with silica (SC), as shown in Figure 1a. This finding aligns with prior research by Fujiwara *et al.* [35] and is likely due to high hydrogen uptake in the bound rubber formed by interactions between the matrix rubber and CB particles. For FKM and HNBR, an interesting trend emerges: carbon black (CB)-filled compounds exhibit slightly higher equilibrium hydrogen content but generally lower diffusion coefficients compared to their unfilled or silica-coated (SC)-filled counterparts. This correlation can be attributed to two key factors: (1) CB particles create a more complex and convoluted path for hydrogen molecules, increasing the diffusion path length and slowing gas transport; (2) the presence of CB filler restricts rubber chain motion, reducing the free volume in the rubber matrix and making it more difficult for gas molecules to diffuse. [36-38] However, this trend is not observed in EPDM or NBR. We attribute this deviation to the presence of an oil-based plasticizer and the specific vulcanization system used. Both EPDM and NBR were vulcanized with sulfur and zinc oxide, which we previously reported as potentially contributing to void initiation at the zinc oxide surface upon exposure to high-pressure hydrogen, thereby altering the diffusion behavior. [39]

A non-linear swelling behavior, where most of the elastomer's volume expansion occurred toward the end of decompression and post-decompression rather than progressing linearly throughout the decompression phase, was first reported in our prior work [24]. In this study, most model elastomers exhibited similar non-linear swelling behavior, except for those with negligible volume swell, as shown in Figures 2-6 for each elastomer type. The volume increase observed at various points during decompression is summarized in Table S2. Generally, all

model elastomers followed a similar swelling rate when 67% of the peak pressure (i.e., a reduction from 90 MPa to 30 MPa) was released. However, as the pressure dropped further, their swelling patterns began to diverge. This suggests that for applications operating primarily at higher pressures (>30 MPa) – such as cascade pressure tanks [40,41] in hydrogen refueling stations – these elastomers may be considered identical in terms of volume swelling behavior. As expected, all unfilled compounds exhibited significantly greater maximum volume expansion compared to the filled systems, due to the increased tortuosity and reduced polymer chain mobility induced by the fillers.

A closer examination of Figure 2 reveals that the four model EPDM compounds exhibit increasing volume expansion rates during decompression from 20 MPa to atmospheric pressure, in the following order: EPDM-CB-nP ≤ EPDM-F-P ≤ EPDM-nF-nP < EPDM-nF-P. This trend reflects the combined effects of mechanical reinforcement and hydrogen diffusivity. Specifically, the storage modulus at 25°C ranks as EPDM-F-P > EPDM-CB-nF > EPDM-nF-nP ≥ EPDM-nF-nP (Table 1), while the diffusion coefficients follow the order: EPDM-nF-P > EPDM-F-P > EPDM-CB-nP ≥ EPDM-nF-nP (Figure 1b). In contrast, all NBR compounds showed similar volume increases over the same pressure range, except for NBR-nF-P, which exhibited accelerated swelling (Figure 3). Given the comparable diffusion coefficients among these NBR compounds, the difference is likely governed by plasticizer solubility. As demonstrated in our prior work [15], the plasticizer interacts less strongly with NBR than with EPDM, contributing to this divergence.

For FKM71 (Figure 4) and FKM65 (Figure 5), all filled compounds demonstrated improved resistance to rapid hydrogen decompression compared to their unfilled counterparts. This is attributed to their significantly higher bulk moduli (e.g., FKM71-CB: 50.02 MPa vs. FKM71-nF:

1.78 MPa). Interestingly, FKM71-SC exhibited greater volume expansion than other filled FKM71 systems – though still less than the unfilled compound – and also exceeded its FKM65 counterpart. This may stem from hydrogen disrupting the silica-fluorine interactions in FKM, with higher fluorine content amplifying the effect [42,43]. Furthermore, compounds filled with both CB and SC (i.e., FKM71-F and FKM65-F) showed identical swelling behavior despite their different fluorine contents, suggesting CB exerts a stronger influence on swelling resistance than SC in this context. As shown in Figure 6, HNBR-nF and HNBR-CB demonstrated slightly faster volume increases compared to HNBR-SC and HNBR-F, although this trend did not align with their maximum volume increases. Instead, maximum swelling followed the order: HNBR-nF > HNBR-F > HNBR-SC > HNBR-CB. This discrepancy may be due to the inherently low hydrogen uptake in these compounds, which diminishes the impact of hydrogen diffusion on final swelling. In this case, the maximum volume increases generally showed an inverse correlation with storage modulus. The exception was observed for HNBR-F and HNBR-SC: although HNBR-F exhibited a higher storage modulus than HNBR-SC, it also swelled more. This discrepancy is likely attributable to the different interfacial interactions of carbon black and silica with the elastomer matrix, as well as the local heterogeneity introduced in the blended filler system.

Figure 7 presents an overview and cross-species comparison of the swelling behavior of all model compounds under identical hydrogen test conditions. As previously discussed, at 10 MPa (i.e., with 89% of the original pressure released and 11% remaining), the volume increase among the various elastomer compounds ranges from 4% to 20%, indicating relatively modest differences in their swelling behavior under these conditions. This behavior is likely attributed to gas expansion caused by the rapid pressure drop, which induces increased stress and strain

within the free volume and voids of the rubber matrix, leading to swelling. However, this increase in internal stress and strain does not exceed the elastic limit of the materials, thereby constraining further swelling. The swelling behavior of these model compounds began to diverge more noticeably when the pressure was reduced to 1 MPa or fully released. Most of the filled FKM compounds (i.e., FKM71-CB, FKM71-F, FKM65-CB, FKM65-SC, and FKM65-F) exhibited significantly lower volume swell (4-6%) compared to model EPDM, NBR, and HNBR materials. Notably, these FKM compounds did not show any additional volume increase upon complete pressure release from 1 MPa. This behavior correlates well with their relatively high storage modulus values and low hydrogen diffusion coefficients.

To further investigate the relationship between hydrogen transport properties and elastomer swelling behavior, the maximum volume increase of all model systems was plotted against hydrogen equilibrium content and diffusion coefficient, as shown in Figure 8. At first glance, no clear correlation is observed when both filled and unfilled compounds are considered together. However, a notable trend emerges – filled materials (red dots in Figure 8) generally exhibit lower volume swell compared to unfilled compounds (black dots), regardless of their hydrogen equilibrium content or diffusion coefficient. This trend is expected, as swelling behavior in elastomers results from a complex interplay of factors, including bulk modulus, transport properties, filler type and loading, crosslink density, and other formulation-specific variables. To further refine the analysis, all data points corresponding to unfilled compounds were excluded, and the remaining data from Figure 8 were replotted as Figure 9, where linear regression was applied to assess potential correlations between hydrogen transport properties and elastomer swelling behavior. Interestingly, a weak linear correlation was observed between maximum volume increase and hydrogen equilibrium content ($R = 0.67$, $R^2 = 0.45$), suggesting that

elastomers with higher hydrogen uptake tend to exhibit greater swelling. The relatively low correlation values can largely be attributed to the two FKM series, likely due to their high modulus. In these cases, modulus appears to play a more dominant role in governing swelling behavior than hydrogen uptake. In contrast, the diffusion coefficient showed a stronger linear correlation with maximum volume increase ($R = 0.91$, $R^2 = 0.82$), indicating that diffusivity has a greater influence on elastomer swelling behavior than equilibrium hydrogen content.

The swelling behavior of all model elastomers was further evaluated by examining correlations between various material properties and maximum swelling percentage, as illustrated in Figure 10. To better understand the interdependence of these factors, both Pearson and Spearman correlation coefficients were employed. Pearson correlation was used to capture the strength and direction of linear relationships, while Spearman correlation assessed monotonic trends in non-linear data. Correlation values range from –1 to +1, with coefficients above ±0.70 indicating strong correlations and values between ±0.30 and ±0.70 suggesting moderate relationships. Figure 10(a) and (b) present the correlations between elastomer properties and maximum swelling, whereas Figure 10(c) and (d) show the correlations among the properties themselves. Our analysis revealed several key trends. In filled elastomers, maximum volume swell exhibited strong negative correlations with Young's modulus, storage modulus, and hardness (Figure 10(a)). For unfilled elastomers, these properties showed weaker but still negative correlations with swelling (Figure 10(b)). These results indicate that higher modulus and hardness—typically associated with increased crosslink density, stiffer networks, and greater resistance to deformation—restrict swelling. Density also showed negative correlations with swelling in both filled and unfilled elastomers, suggesting that tighter molecular packing reduces available free volume for hydrogen penetration.

In contrast, the hydrogen diffusion coefficient displayed a strong positive correlation with maximum swelling in filled systems (Figure 10(a)). This trend implies that elastomers susceptible to swelling also permit faster hydrogen transport, likely due to network loosening or void formation that increases molecular mobility. For unfilled elastomers, the same trends were observed but with generally weaker correlations, indicating the need for larger datasets to strengthen these insights. The heatmaps in Figure 10(c) and (d) highlight the intrinsic interconnections among elastomer properties. In filled systems, modulus, hardness, and crosslink density were strongly and positively correlated, collectively acting to limit swelling. For unfilled elastomers (Figure 10(d)), correlations were weaker overall, except for the strong positive relationships between hardness, Young's modulus, and storage modulus, and the strong negative correlation between Young's modulus and hydrogen diffusion coefficients. Taken together, these findings underscore the critical role of microstructural characteristics and mechanical properties in governing elastomer swelling behavior. Understanding these relationships provides a foundation for rational formulation design, supports the development of predictive models using larger datasets and machine learning, and helps define viable design spaces for advanced elastomer solutions tailored to specific applications.

CONCLUSIONS

This study systematically evaluated the swelling behavior of model elastomers under high-pressure hydrogen conditions, revealing key structure–property relationships that govern elastomer performance. Across all tested materials – EPDM, NBR, FKM, and HNBR – filled compounds consistently exhibited reduced swelling compared to unfilled systems, primarily due to increased stiffness, reduced chain mobility, and lower hydrogen diffusivity. Carbon black, in

particular, proved effective at limiting volume expansion. Correlation analysis provided deeper insight into these trends — swelling was suppressed by higher modulus, hardness, and density, while the hydrogen diffusion coefficient showed the strongest positive correlation, especially in filled elastomers; heatmaps confirmed that stiffness-related properties act collectively to limit swelling, with weaker inter-property relationships in unfilled systems.

These findings highlight the complex interplay of mechanical, transport, and formulation-specific factors that influence elastomer performance in hydrogen environments. The insights gained provide a foundation for the rational design of elastomers with tailored resistance to rapid gas decompression, and they support the development of predictive models to guide material selection for hydrogen infrastructure applications.

ACKNOWLEDGEMENTS

This work was fully supported by the U.S. Department of Energy (USDOE), Office of Energy Efficiency and Renewable Energy (EERE), Hydrogen and Fuel Cells Technologies Office (HFTO). Pacific Northwest National Laboratory is operated by Battelle Memorial Institute for the USDOE under Contract Number DE-AC05-76RL01830. We thank Kyushu University for their contribution to the development and formulation of all model compounds used in this work.

DECLARATION OF INTEREST STATEMENT

The views and opinions of the authors expressed herein do not necessarily state or reflect those of the United States Government or any agency thereof. Neither the United States

Government nor any agency thereof, nor any of their employees, makes any warranty, expressed or implied, or assumes any legal liability or responsibility for the accuracy, completeness, or usefulness of any information, apparatus, product, or process disclosed, or represents that its use would not infringe privately owned rights.

REFERENCES

[1] Bonsu, N. O. (2020). Towards a circular and low-carbon economy: Insights from the transitioning to electric vehicles and net zero economy. *Journal of Cleaner Production*, 256, 120659.
[2] Rogelj, J., Geden, O., Cowie, A., & Reisinger, A. (2021). Three ways to improve net-zero emissions targets. *Nature*, 591(7850), 365-368.
[3] Singh, S., Jain, S., Venkateswaran, P. S., Tiwari, A. K., Nouni, M. R., Pandey, J. K., & Goel, S. (2015). Hydrogen: A sustainable fuel for future of the transport sector. *Renewable and sustainable energy reviews*, 51, 623-633.
[4] Tashie-Lewis, B. C., & Nnabuife, S. G. (2021). Hydrogen production, distribution, storage and power conversion in a hydrogen economy-a technology review. *Chemical Engineering Journal Advances*, 8, 100172.
[5] Ahad, M. T., Bhuiyan, M. M. H., Sakib, A. N., Becerril Corral, A., & Siddique, Z. (2023). An overview of challenges for the future of hydrogen. *Materials*, *16*(20), 6680.
[6] Meda, U. S., Bhat, N., Pandey, A., Subramanya, K. N., & Raj, M. L. A. (2023). Challenges associated with hydrogen storage systems due to the hydrogen embrittlement of high strength steels. *International Journal of Hydrogen Energy*, *48*(47), 17894-17913.
[7] Le, T. T., Sharma, P., Bora, B. J., Tran, V. D., Truong, T. H., Le, H. C., & Nguyen, P. Q. P. (2024). Fueling the future: A comprehensive review of hydrogen energy systems and their challenges. *International Journal of Hydrogen Energy*, *54*, 791-816.
[8] Zheng, Y., Tan, Y., Zhou, C., Chen, G., Li, J., Liu, Y., ... & Zhang, G. (2020). A review on effect of hydrogen on rubber seals used in the high-pressure hydrogen infrastructure. *International Journal of Hydrogen Energy*, 45(43), 23721-23738.
[9] Balasooriya, W., Clute, C., Schrittesser, B., & Pinter, G. (2022). A review on applicability, limitations, and improvements of polymeric materials in high-pressure hydrogen gas atmospheres. *Polymer reviews*, 62(1), 175-209.
[10] Alvine, K. J., Kafentzis, T. A., Pitman, S. G., Johnson, K. I., Skorski, D., Tucker, J. C., ... & Dahl, M. E. (2014). An in situ tensile test apparatus for polymers in high pressure hydrogen. *Review of Scientific Instruments*, 85(10).
[11] Castagnet, S., Grandidier, J. C., Comyn, M., & Benoît, G. (2012). Mechanical testing of polymers in pressurized hydrogen: tension, creep and ductile fracture. *Experimental mechanics*, *52*(3), 229-239.
[12] Wang, J. J. A., Ren, F., Tan, T., & Liu, K. (2015). The development of in situ fracture toughness evaluation techniques in hydrogen environment. *International Journal of hydrogen energy*, *40*(4), 2013-2024.
[13] Duranty, E. R., Roosendaal, T. J., Pitman, S. G., Tucker, J. C., Owsley, S. L., Suter, J. D., & Alvine, K. J. (2017). An in situ tribometer for measuring friction and wear of polymers in a high pressure hydrogen environment. *Review of Scientific Instruments*, 88(9).
[14] Duranty, E. R., Roosendaal, T. J., Pitman, S. G., Tucker, J. C., Owsley Jr, S. L., Suter, J. D., & Alvine, K. J. (2018). In situ high pressure hydrogen tribological testing of common polymer materials used in the hydrogen delivery infrastructure. *Journal of Visualized Experiments: JoVE*, (133), 56884.
[15] Kuang, W., Bennett, W. D., Roosendaal, T. J., Arey, B. W., Dohnalkova, A., Petrossian, G., & Simmons, K. L. (2021). In situ friction and wear behavior of rubber materials incorporating various fillers and/or a plasticizer in high-pressure hydrogen. *Tribology International*, 153, 106627.
[16] Theiler, G., Cano Murillo, N., & Hausberger, A. (2024). Effect of hydrogen pressure on the fretting behavior of rubber materials. *Lubricants*, *12*(7), 233.
[17] Choi, B. L., Choi, M. C., Jeon, S. K., bong Baek, U., & Choi, B. H. (2025). In situ wear test of acrylonitrile butadiene rubber in a low pressure hydrogen environment. *Polymer Testing*, *142*, 108683.

[18] Jung, J. K., Jeon, S. K., Kim, K. T., Lee, C. H., Baek, U. B., & Chung, K. S. (2019). Impedance spectroscopy for in situ and real-time observations of the effects of hydrogen on nitrile butadiene rubber polymer under high pressure. *Scientific Reports*, *9*(1), 13035.
[19] Lee, J. H. (2025). Development of In-situ Hydrogen Permeation Measurement Technology Based on Manometric Analysis of Polymer Specimen under High Pressure Hydrogen Environment. *Applied Science and Convergence Technology*, *34*(3), 108-114.
[20] Kane-Diallo, O., Castagnet, S., Nait-Ali, A., Benoit, G., & Grandidier, J. C. (2016). Time-resolved statistics of cavity fields nucleated in a gas-exposed rubber under variable decompression conditions–support to a relevant modeling framework. *Polymer Testing*, 51, 122-130.
[21] Ono, H., Nait-Ali, A., Kane Diallo, O., Benoit, G., & Castagnet, S. (2018). Influence of pressure cycling on damage evolution in an unfilled EPDM exposed to high-pressure hydrogen. *International Journal of Fracture*, 210, 137-152.
[22] Castagnet, S., Mellier, D., Nait-Ali, A., & Benoit, G. (2018). In-situ X-ray computed tomography of decompression failure in a rubber exposed to high-pressure gas. *Polymer testing*, *70*, 255-262.
[23] Castagnet, S., Nait-Ali, A., & Ono, H. (2019). Effect of pressure cycling on decompression failure in EPDM exposed to high-pressure hydrogen. In *Constitutive models for rubber XI* (pp. 169-172). CRC Press.
[24] Kuang, W., Nickerson, E. K., Li, D., Clelland, D. T., Seffens, R. J., Ramos, J. L., & Simmons, K. L. (2024). An in-situ view cell system for investigating swelling behavior of elastomers upon high-pressure hydrogen exposure. *International Journal of Hydrogen Energy*, *71*, 1317-1325.
[25] Yamabe, J., & Nishimura, S. (2009). Influence of fillers on hydrogen penetration properties and blister fracture of rubber composites for O-ring exposed to high-pressure hydrogen gas. *International Journal of Hydrogen Energy*, *34*(4), 1977-1989.
[26] Yamabe, J., Nakao, M., Fujiwara, H., & Nishimura, S. (2008). Influence of fillers on hydrogen penetration properties and blister fracture of EPDM composites exposed to 10 MPa hydrogen gas. *Nihon Kikai Gakkai Ronbunshu, A Hen/Transactions Of The Japan Society Of Mechanical Engineers, Part A*, *74*(743), 971-981.
[27] Ono, H., Fujiwara, H., & Nishimura, S. (2018). Penetrated hydrogen content and volume inflation in unfilled NBR exposed to high-pressure hydrogen–What are the characteristics of unfilled-NBR dominating them? *International Journal of Hydrogen Energy*, *43*(39), 18392-18402.
[28] Almeida, R., & Hood, E. S. (1992). Nonequilibrium dynamics in thermal desorption. *The Journal of Physical Chemistry*, *96*(7), 3086-3092.
[29] Castro, F. J., & Meyer, G. (2002). Thermal desorption spectroscopy (TDS) method for hydrogen desorption characterization (I): theoretical aspects. *Journal of alloys and Compounds*, *330*, 59-63.
[30] Demarez, A. L., Hock, A. G., & Meunier, F. A. (1954). Diffusion of hydrogen in mild steel. *Acta Metallurgica*, *2*(2), 214-223.
[31] Fujiwara, H., Ono, H., Onoue, K., & Nishimura, S. (2020). High-pressure gaseous hydrogen permeation test method-property of polymeric materials for high-pressure hydrogen devices (1)-. *International Journal of Hydrogen Energy*, *45*(53), 29082-29094.
[32] Fujiwara, H., Ono, H., Ohyama, K., Kasai, M., Kaneko, F., & Nishimura, S. (2021). Hydrogen permeation under high pressure conditions and the destruction of exposed polyethylene-property of polymeric materials for high-pressure hydrogen devices (2)-. *International Journal of Hydrogen Energy*, *46*(21), 11832-11848.
[33] Kanesugi, H., Ohyama, K., Fujiwara, H., & Nishimura, S. (2023). High-pressure hydrogen permeability model for crystalline polymers. *International Journal of Hydrogen Energy*, *48*(2), 723-739.
[34] Schober, P., Boer, C., & Schwarte, L. A. (2018). Correlation coefficients: appropriate use and interpretation. *Anesthesia & analgesia*, *126*(5), 1763-1768

[35] Fujiwara, H., Ono, H., & Nishimura, S. (2022). Effects of fillers on the hydrogen uptake and volume expansion of acrylonitrile butadiene rubber composites exposed to high pressure hydrogen:-Property of polymeric materials for high pressure hydrogen devices (3)-. *International Journal of Hydrogen Energy*, *47*(7), 4725-4740.
[36] Yamabe, J., & Nishimura, S. (2011). Influence of carbon black on decompression failure and hydrogen permeation properties of filled ethylene-propylene–diene–methylene rubbers exposed to high-pressure hydrogen gas. *Journal of applied polymer science*, *122*(5), 3172-3187.
[37] Jung, J. K., Lee, C. H., Son, M. S., Lee, J. H., Baek, U. B., Chung, K. S., ... & Bae, J. W. (2022). Filler effects on H2 diffusion behavior in nitrile butadiene rubber blended with carbon black and silica fillers of different concentrations. *Polymers*, *14*(4), 700.
[38] Zhou, C., Yan, X., Zheng, Y., Xia, L., Huang, Y., Liu, X., ... & Hua, Z. (2024). Hydrogen permeation behavior and mechanisms in nitrile butadiene rubber composites for hydrogen sealing. *Polymer Degradation and Stability*, *229*, 110969.
[39] Kuang, W., Arey, B. W., Dohnalkova, A. C., Kovarik, L., Mills, B., Menon, N. C., ... & Simmons, K. L. (2023). Multi-scale imaging of high-pressure hydrogen induced damage in EPDM rubber using X-ray microcomputed tomography, helium-ion microscopy and transmission electron microscopy. *International Journal of Hydrogen Energy*, 48(23), 8573-8587.
[40] Xiao, L., Chen, J., Wu, Y., Zhang, W., Ye, J., Shao, S., & Xie, J. (2021). Effects of pressure levels in three-cascade storage system on the overall energy consumption in the hydrogen refueling station. *International journal of hydrogen energy*, *46*(61), 31334-31345.
[41] Park, B. H., & Joe, C. H. (2024). Investigation of configuration on multi-tank cascade system at hydrogen refueling stations with mass flow rate. *International Journal of Hydrogen Energy*, *49*, 1140-1153.
[42] Zhang, H., Zhao, L., Zhang, C., Xu, Y., & Jia, W. (2023). Study on the interaction between fluoroelastomer and silica: Characterizations. *Polymer Engineering & Science*, *63*(12), 4249-4261.
[43] Khanra, S., Ganguly, D., Ghorai, S. K., Goswami, D., & Chattopadhyay, S. (2020). The synergistic effect of fluorosilicone and silica towards the compatibilization of silicone rubber and fluoroelastomer based high performance blend. *Journal of Polymer Research*, *27*, 1-17.

TABLES

Table 1. Compositions of Model EPDM and NBR Elastomers

Unit: parts per hundred rubber (phr)	EPDM-nF-nP	EPDM-nF-P	EPDM-CB-nP	EPDM-F-P	NBR-nF-nP	NBR-nF-P	NBR-CB-nP	NBR-F-P
Base Material	Esprene505*	Esprene505*	Esprene505*	Esprene505*	Nipol 1042*	Nipol 1042*	Nipol 1042*	Nipol 1042*
Base Rubber	100	100	100	100	100	100	100	100
Stearic Acid	1	1	1	1	1	1	1	1
Zinc Oxide	5	5	5	5	5	5	5	5
Sulfur	1.5	1.5	1.5	1.5	1.5	1.5	1.5	1.5
MBTS [a]	1.5	1.5	1.5	1.5	1.5	1.5	1.5	1.5
TMTD [a]	0.7	0.7	0.7	0.7	0.5	0.5	0.5	0.5
DOS [b]	-	10	-	10	-	10	-	10
Carbon Black (N330)	-	-	25	21	-	-	25	23
Silica (Nipsil VN3)	-	-	-	25	-	-	-	28

*Esprene 505 (Sumitomo Chemical): ethylene 50%, propylene 40%, 5-ethylidene-2-norbornene (ENB) 10%; Nipol 1042 (Zeon Corporation): medium high nitrile rubber, acrylonitrile content 33.5%

[a] Accelerators – MBTS:2,2′-benzothiazyl disulfide, TMTD: bis(dimethylthiocarbamoyl) disulfide

[b] Plasticizer – DOS: dioctyl sebacate

[c] Measured through dynamic mechanical analysis using a strain of 1%, a frequency of 1 Hz, and an axial tension of 1 N.

Table 2. Compositions of Model FKM Elastomers

Unit: parts per hundred rubber (phr)	FKM71-nF	FKM71-CB	FKM71-SC	FKM71-F	FKM65-nF	FKM65-CB	FKM65-SC	FKM65-F
Base Material	Daikin G902	Daikin G902	Daikin G902	Daikin G902	Daikin LT304	Daikin LT304	Daikin LT304	Daikin LT304
Features	Fluorine content of 71%, unfilled	Fluorine content of 71%, filled with carbon black	Fluorine content of 71%, filled with silica	Fluorine content of 71%, filled with both	Fluorine content of 65%, unfilled	Fluorine content of 65%, filled with carbon black	Fluorine content of 65%, filled with silica	Fluorine content of 65%, filled with both
Base Rubber	100	100	100	100	100	100	100	100
Trially Isocyanurate	2	2	2	2	2	2	2	2
Peroxide (25B-40)	1.5	3.8	1.5	1.5	1.5	1.5	1.5	1.5
Carbon Black (N330)	-	30	-	8	-	40	-	10
Silica (Nipsil VN3)	-	-	20	16	-	-	22	20

Table 3. Compositions of Model HNBR Elastomers

Unit: parts per hundred rubber (phr)	HNBR-nF	HNBR-CB	HNBR-SC	HNBR-F
Base Material	Zetpol 3300	Zetpol 3300	Zetpol 3300	Zetpol 3300
Features	Acrylonitrile (AN) content 23.6% I value 10	AN 23.6% I value 10	AN 23.6% I value 10	AN 23.6% I value 10
Base Rubber	100	100	100	100
Perbutyl Peroxide (40%)	8	8	8	8
Carbon Black (N330)	-	86	-	22
Silica (Nipsil VN3)	-	-	55	44

Table 4. Material Properties of Model Elastomers

	Density (g/cm^3)	Storage Modulus at 25°C (MPa)	Crosslink Density (mol/cm^3)	Hardness (Shore A)	Young's Modulus (MPa)
EPDM-nF-nP	0.921	1.30	0.00292144	55.3	3.716
EPDM-nF-P	0.919	1.17	0.003276178	48.3	2.935
EPDM-CB-nP	1.01	5.16	0.00565139	67.2	6.378
EPDM-F-P	1.07	7.39	0.008307386	72	9.133
NBR-nF-nP	1.03	1.43	0.000159949	51	3.402
NBR-nF-P	1.01	1.14	0.00012409	43.4	2.089
NBR-CB-nP	1.11	7.84	4.01937E-05	66	4.833
NBR-F-P	1.18	6.24	2.32095E-05	65.8	5.514
FKM71-nF	1.9	1.78	0.0283	55.5	3.924
FKM71-CB	1.85	50.02	0.0226	87.5	33.147
FKM71-SC	1.88	21.67	0.0172	81	23.751
FKM71-F	1.89	29.86	0.0184	80.5	23.512
FKM65-nF	1.79	1.41	0.0288	53.3	4.4578
FKM65-CB	1.79	43.43	0.0228	84.5	25.891

FKM65-SC	1.82	14.46	0.0212	82	21.027
FKM65-F	1.83	29.44	0.0204	86	29.944
HNBR-nF	0.98	1.12	0.1808	48.6	3.485
HNBR-CB	1.23	40.29	0.5089	79	20.110
HNBR-SC	1.19	17.11	0.0306	82	19.097
HNBR-F	1.21	24.12	0.0728	81.5	22.447

FIGURES

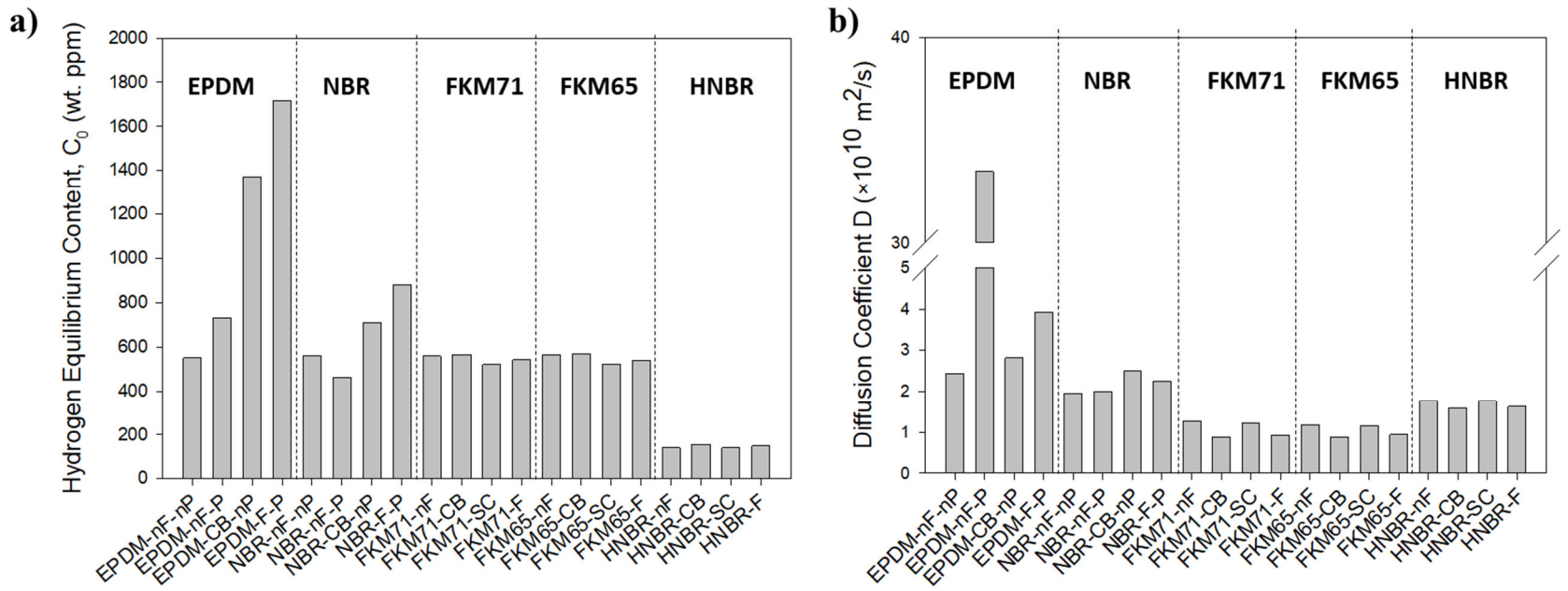

Figure 1. a) Hydrogen equilibrium contents and **b)** diffusion coefficients of all model elastomers exposed to hydrogen gas at 90 MPa and room temperature (~22°C).

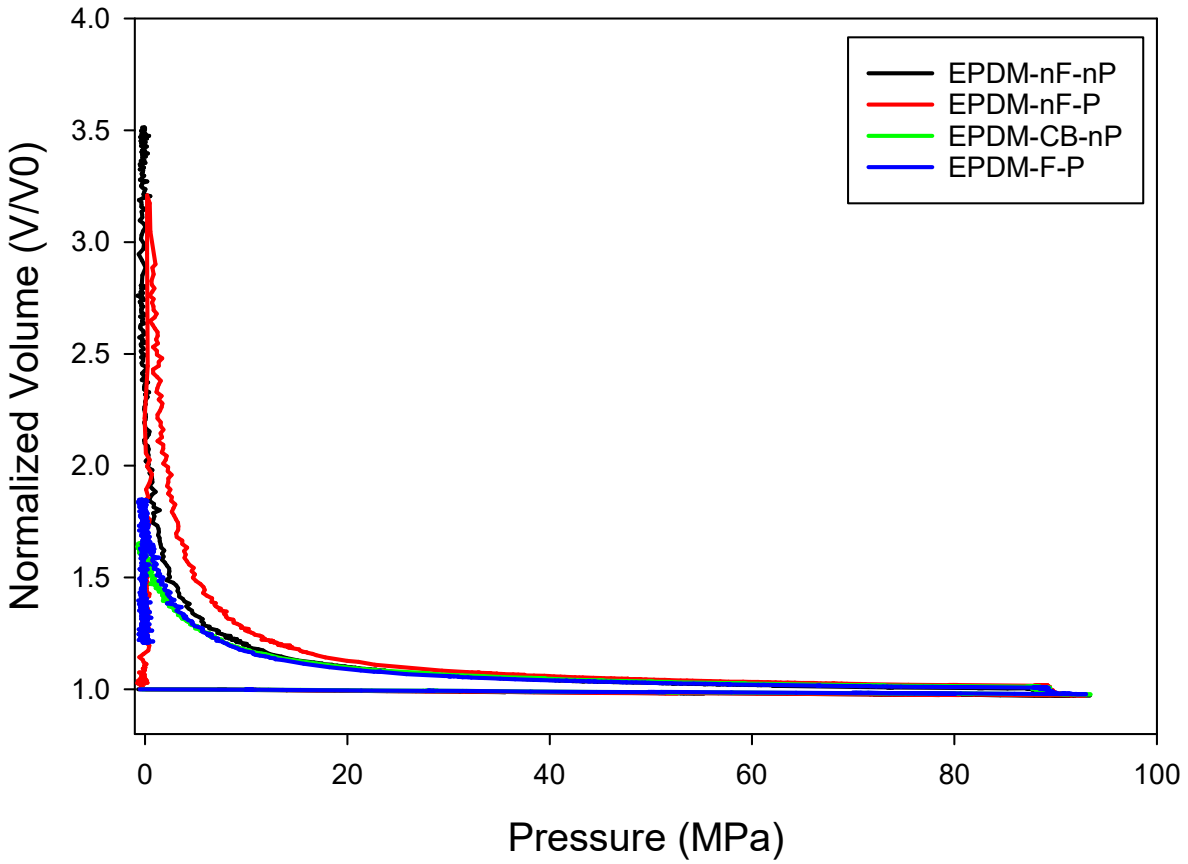

Figure 2. Normalized volume (V/V_0)-pressure curves for model EPDM elastomers during the entire course of a high-pressure hydrogen test.

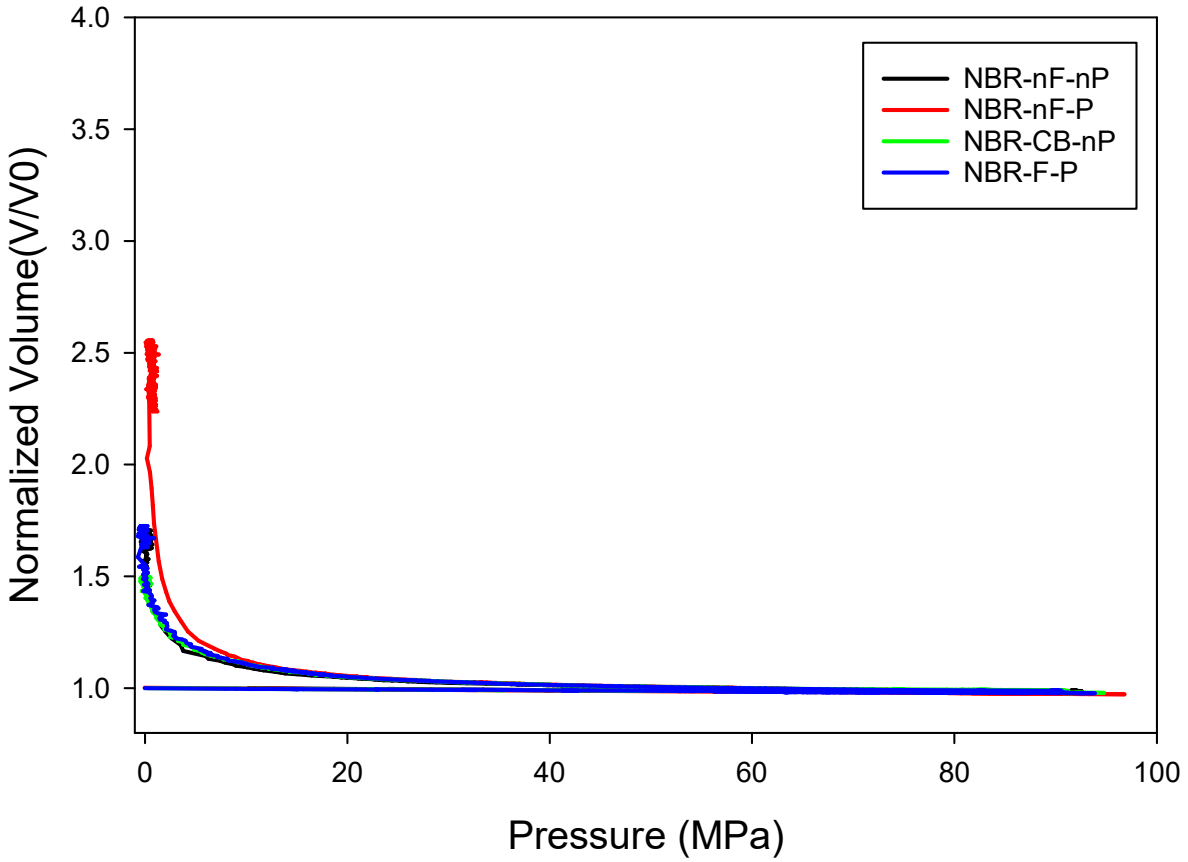

Figure 3. Normalized volume (V/V_0)-pressure curves for model NBR elastomers during the entire course of a high-pressure hydrogen test.

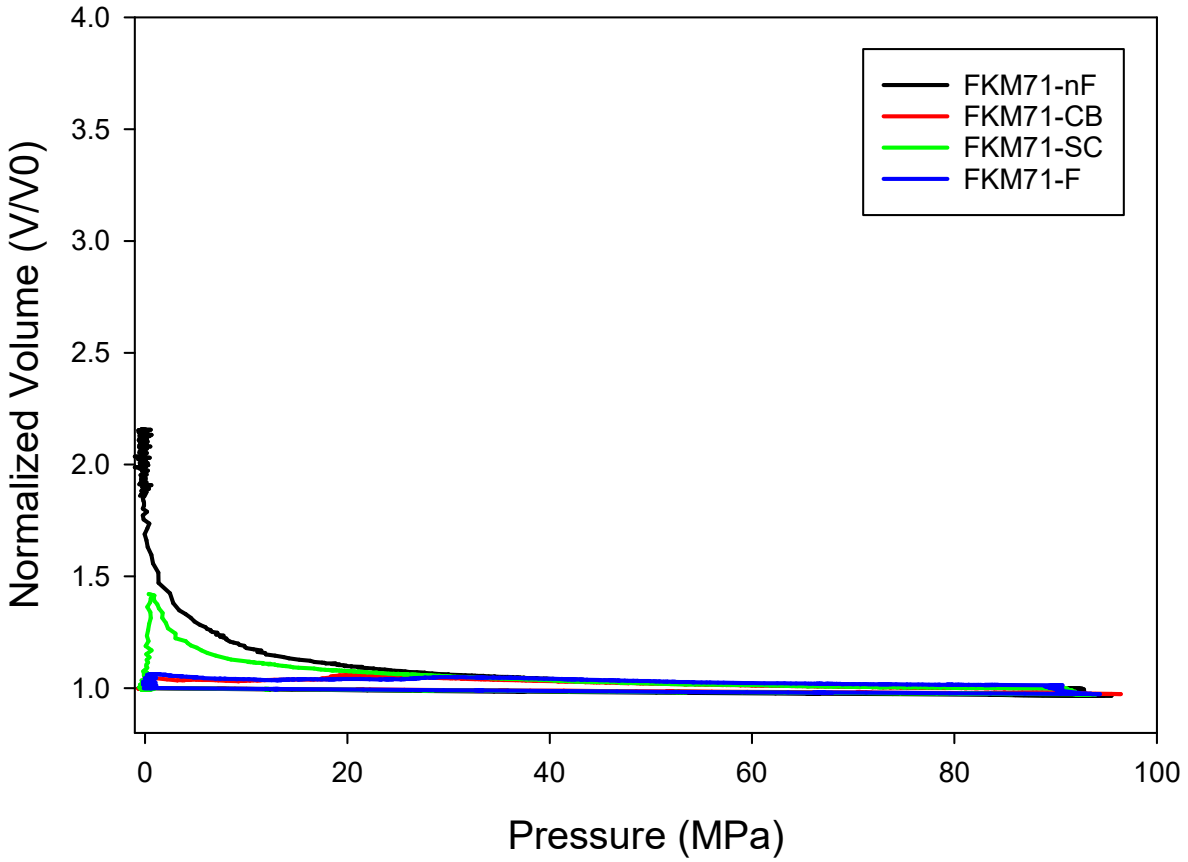

Figure 4. Normalized volume (V/V_0)-pressure curves for model FKM71 elastomers during the entire course of a high-pressure hydrogen test.

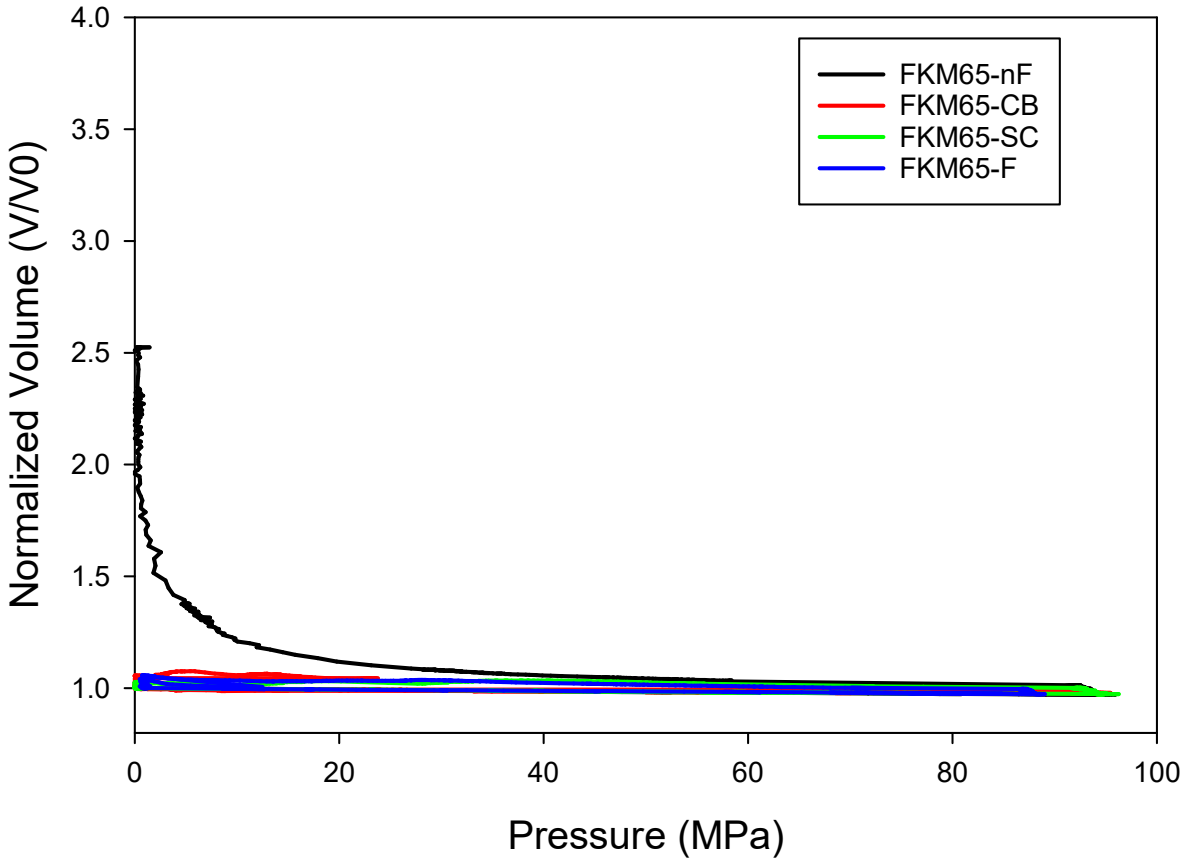

Figure 5. Normalized volume (V/V_0)-pressure curves for model FKM65 elastomers during the entire course of a high-pressure hydrogen test.

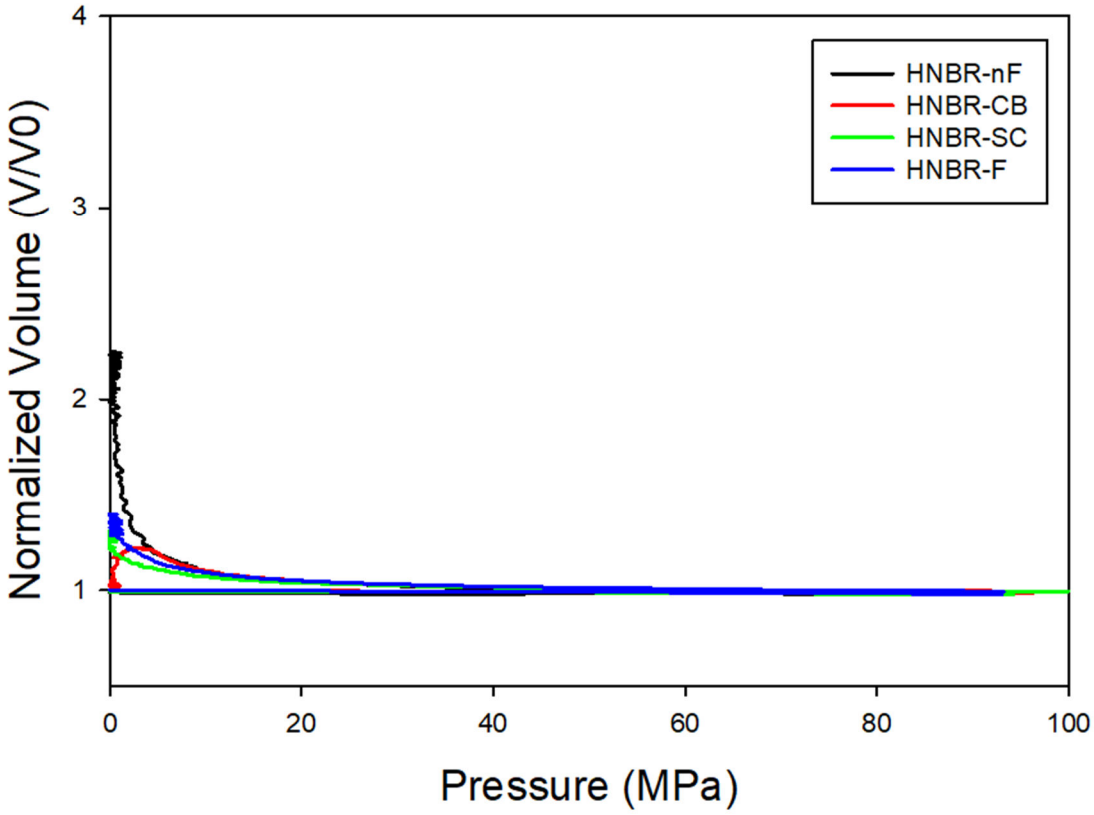

Figure 6. Normalized volume (V/V_0)-pressure curves for model HNBR elastomers during the entire course of a high-pressure hydrogen test.

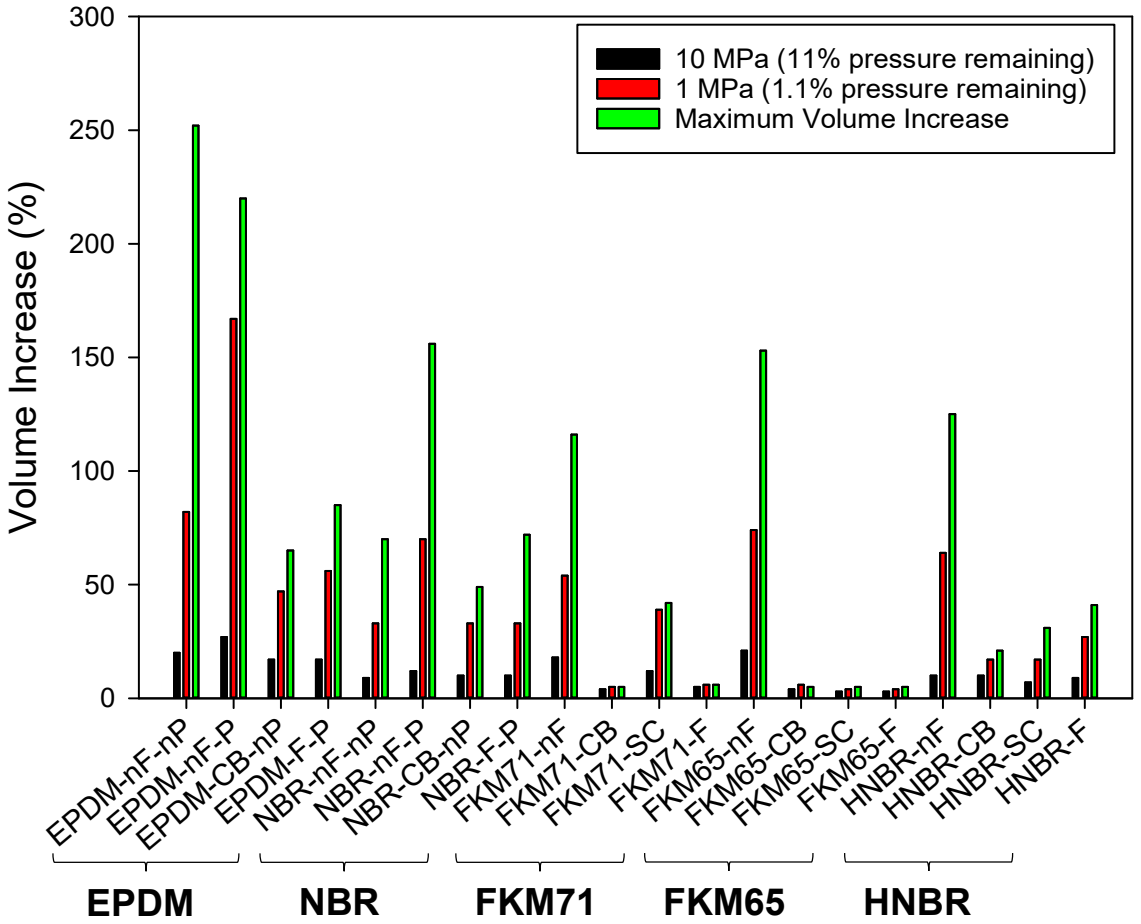

Figure 7. Volume increase (%) of model elastomers at different pressure levels during gas decompression. Black bars indicate the volume increase at 10 MPa (11% of peak pressure remaining), while red bars represent the volume increase at 1 MPa (1.1% of peak pressure remaining). Green bars denote the maximum volume increase observed for each elastomer throughout the high-pressure hydrogen test.

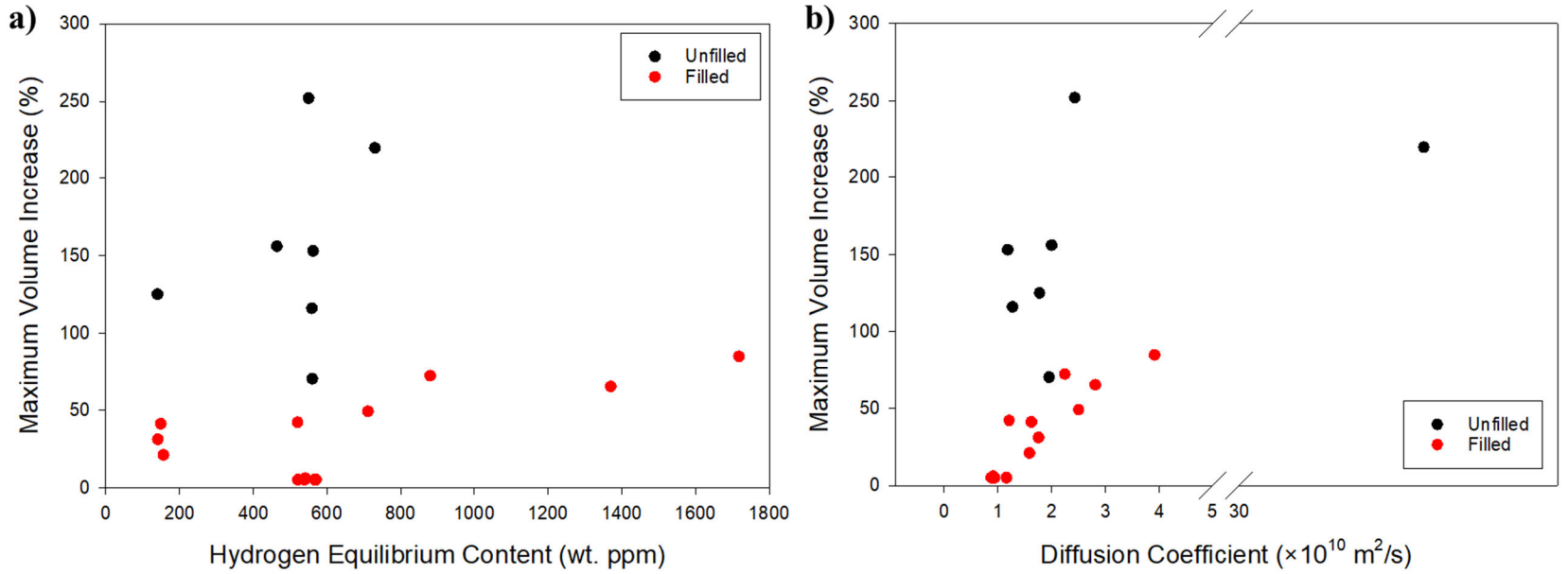

Figure 8. a) Maximum volume increase vs. hydrogen equilibrium content and **b)** maximum volume increase vs. diffusion coefficient for unfilled (black) and filled (red) model elastomers.

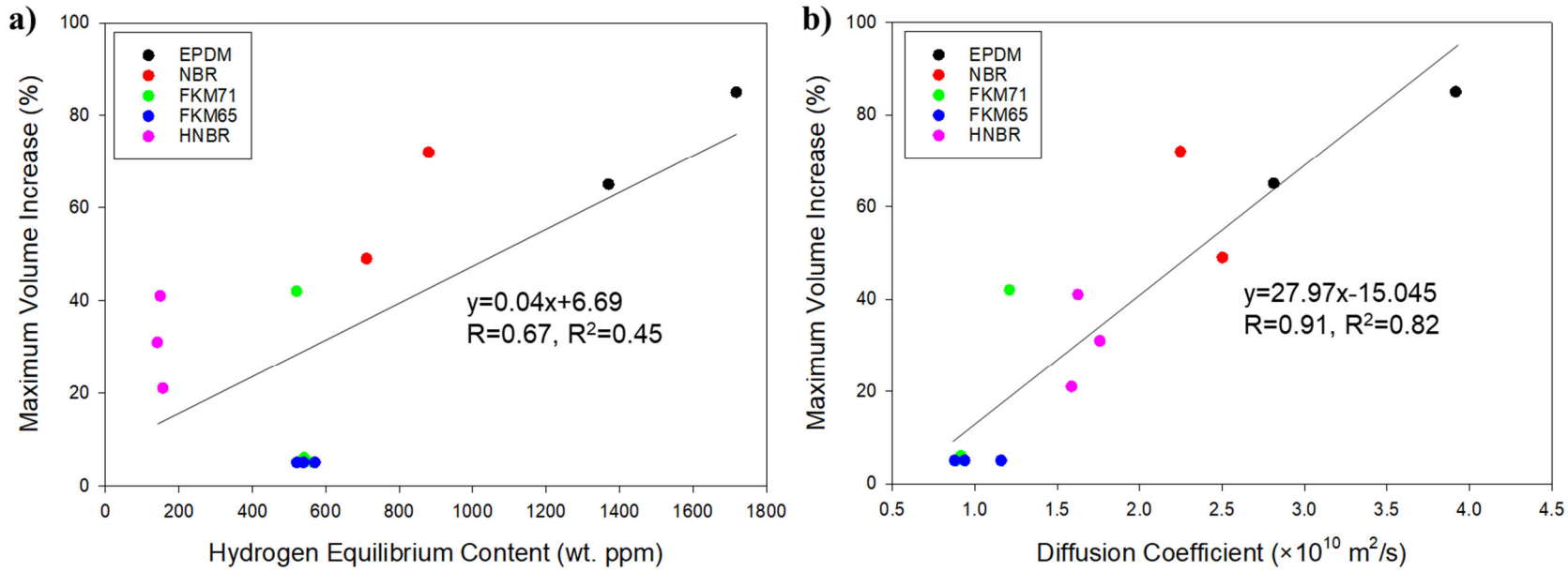

Figure 9. a) Maximum volume increase vs. hydrogen equilibrium content and **b)** maximum volume increase vs. diffusion coefficient for all model elastomers: EPDM (black), NBR (red), FKM71 (green), FKM65 (blue), and HNBR (purple). Black lines represent linear regression fits for each dataset.

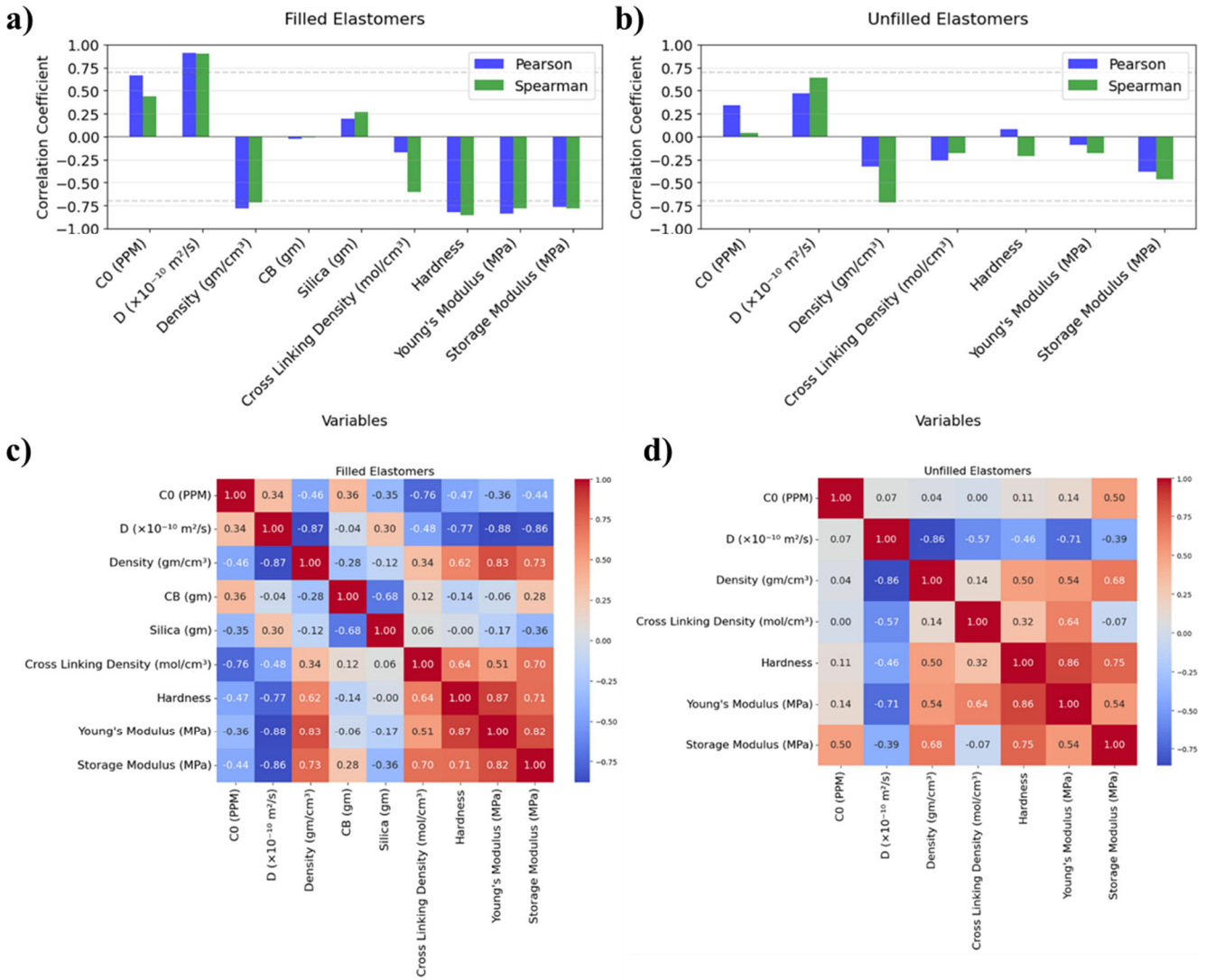

Figure 10. Pearson and Spearman correlation coefficients showing the relationship between filler content and maximum swelling percentage in EPDM, FKM, NBR, and HNBR elastomers for **a)** filled elastomers and **b)** unfilled elastomers. Feature-feature Spearman correlation coefficients for **c)** filled elastomers and **d)** unfilled elastomers.